PNAS
www.pnas.org

Supplementary Information for

Cholesterol in the cargo membrane amplifies tau inhibition of kinesin-1-based transport

Qiaochu Li, James T. Ferrare, Jonathan Silver, John O. Wilson, Luis Arteaga-Castaneda, Weihong Qiu, Michael Vershinin, Stephen J. King, Keir C. Neuman, Jing Xu*

*Jing Xu
Email: jxu8@ucmerced.edu

This PDF file includes:

Other supporting materials for this manuscript include the following:

Supplementary Text

Note 1. Derivation of motile fraction model for binding probabilities below 1 (Eqn. 1 in the main text). We considered the experimental scenario that the number of motors on a cargo follows a Poisson distribution (1, 2). We modeled motile fraction as the weighted sum of the probability that a cargo is carried by at least 1 motor protein, and the probability that at least 1 of these motor proteins binds the microtubule. We assumed that each motor on the cargo binds the microtubule identically and independently. For each preparation of motor-cargo complexes, the mean number of motors on the cargo is $\alpha[M]$, where α is a fitting parameter determined by the motor-cargo attachment strategy, and $[M]$ is the concentration of motors that we used to prepare the motor-cargo complex. The probability that the cargo carries $k = 1, 2, 3, \ldots$ motor(s) is determined by the Poisson probability

$$P(k, \alpha[M]) = \frac{(\alpha[M])^k e^{-\alpha[M]}}{k!}.$$

The probability that at least 1 of these k motors on the cargo binds the microtubule is $1 - (1-p)^k$, where $0 \leq p \leq 1$ is the probability that each motor binds the microtubule within the motile-fraction measurement duration. Summing over all k values, we have

$$\text{Motile fraction} = \sum_{k=1}^{\infty} P(k, \alpha[M]) \cdot (1 - (1-p)^k) = 1 - e^{-p\alpha[M]}.$$

For $p = 1$, our model returns the same expression as that previously developed (1, 2), $1 - e^{-\alpha[M]}$.

Note 2. Derivation of the rate that a motor encounters an open binding site (Fig. 4 and Eqn. 2 in the main text). We modeled the microtubule lattice as a one-dimensional track with periodic binding sites. We then coarse-grained diffusion along this track to derive the time that a motor spends at each binding site before reaching an adjacent binding site. The inverse of this time is the rate that the motor encounters a new binding site. Specifically, we defined each binding site as an open interval of a width much smaller than the periodicity. Under this coarse graining, the motor begins at the center of the binding site; the encounter ends when the motor diffuses to the next binding site centered $\pm\Delta x$ away, where the process repeats itself. Solving the one-dimensional diffusion equation with the initial position of the motor at $x = 0$ and two absorbing boundaries at $\pm\Delta x$, we have

$$P(x,t) = \begin{cases} \frac{1}{\sqrt{4\pi D t}} \cdot \left(e^{-\frac{x^2}{4Dt}} - e^{-\frac{(x-2\Delta x)^2}{4Dt}} \right), & x \geq 0 \\ \frac{1}{\sqrt{4\pi D t}} \cdot \left(e^{-\frac{x^2}{4Dt}} - e^{-\frac{(x+2\Delta x)^2}{4Dt}} \right), & x < 0 \end{cases},$$

where D is the motor's diffusion constant, and $P(x,t)$ is the probability density of finding the motor at position x at time t. The probability that the motor remains within both boundaries for all times up to time t is

$$S(t) = \int_{-\Delta x}^{\Delta x} P(x,t) \cdot dx = 2erf\left(\frac{\Delta x}{2\sqrt{Dt}}\right) - erf\left(\frac{\Delta x}{\sqrt{Dt}}\right),$$

the probability that the motor first reaches either absorbing boundaries at exactly time t is

$$f(t) = -\frac{\partial S(t)}{\partial t} = \frac{\Delta x}{\sqrt{\pi D t^3}} \cdot \left(e^{-\frac{\Delta x^2}{4Dt}} - e^{-\frac{\Delta x^2}{Dt}} \right),$$

and the mean first-passage time of the motor to reach an adjacent binding region is

$$\int_0^{\infty} f(t) \cdot t \cdot dt = \Delta x^2 / D.$$

The inverse of this mean time is the rate that the motor encounters an open binding site, $D/\Delta x^2$.

Supplementary Methods

Immunostaining and Imaging. Flow cells with microtubules were prepared as in optical trapping experiments (Materials and Methods in the main text), with the exception that the microtubules were polymerized with 9% fluorescently labeled tubulin. Briefly, unlabeled tubulin (40 μM) was mixed with an Alexa 488-conjugated tubulin (PurSolutions) at 10:1 ratio and incubated in PM buffer supplemented with 1 mM GTP for 20 min at 37 °C. The assembled microtubules were then incubated with an equal volume of PM buffer supplemented with 40 μM taxol and 1 mM GTP for 20 min at 37°C. Taxol-stabilized microtubules were diluted to 500 nM in microtubule buffer (PMEE buffer supplemented with 10 μM taxol and 1 mM GTP) and incubated with 0 or 90 nM hTau23 in microtubule buffer for 20 min at 37 °C, then diluted to 16 nM in microtubule buffer, and introduced into flow cells for incubation at room temperature for 10 min. The flow cell was then rinsed with microtubule buffer twice for 10 min at room temperature. For immunostaining, microtubules (tau-decorated or tau-free) were first fixed with -20°C methanol for 3 min (3), and immediately washed three times with room-temperature PEM80 buffer (80 mM PIPES, 2 mM $MgCl_2$, 0.5 mM EGTA, pH 6.9) for 5 min each at room temperature. The flow cells were blocked with 4% wt/vol BSA-c (Aurion, reference (4)) in PEM80 buffer for 2.5 h at room temperature, and then incubated with a 1:20 dilution of an Alexa 546-conjugated Tau-13 antibody (Santa Cruz Biotechnology) or a 1:20 dilution of a DyLight 550-conjugated Tau-5 antibody (Novus Biologicals) in 2% wt/vol BSA-c in PEM80 buffer for 2 h at room temperature. Following antibody incubation, the flow cells were washed with PEM80 buffer three times for 10 min each and imaged immediately in PEM80 buffer supplemented with an oxygen-scavenging solution (250 μg/mL glucose oxidase, 30 μg/mL catalase, 4.6 mg/mL glucose). Immunostained microtubules (tau-decorated or tau-free, Fig. S8) were imaged at 100x magnification using an Eclipse Ti-E inverted microscope (Nikon) and an iXon Electron Multiplying CCD camera (Andor). Microtubules were imaged using a FITC filter cube (Chroma). Tau-13 and Tau-5 antibodies were imaged using a TRITC filter cube (Chroma). The resulting images were brightness-adjusted in ImageJ (https://imagej.nih.gov/ij/) and presented in Fig. S8 without further processing.

Supplementary Figures

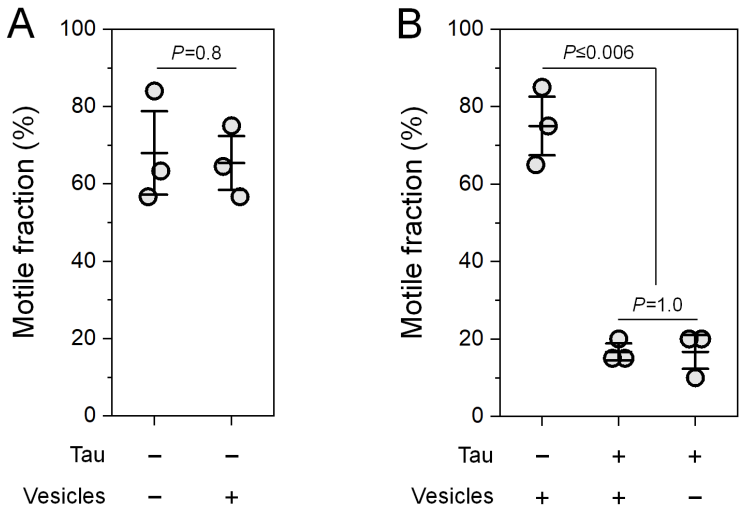

Fig. S1. Preincubating microtubules with motor-free DOPC lipid vesicles does not impact cargo motile fraction. To control for the possibility that the cargo membrane binds and removes tau from the microtubule, microtubules were incubated with excess DOPC lipid vesicles prior to motile-fraction measurements (Materials and Methods in the main text). Membrane-free cargos were tested in order to probe potential membrane effects from vesicle preincubation alone. The concentration of Kif5A was kept constant in order to enable comparisons across experimental conditions. (*A*) Preincubating tau-free microtubules with 100 μM DOPC lipid vesicles (+Vesicles) did not impact cargo motile fraction. Horizontal lines indicate mean and 68% confidence interval. *n* = 3 trials, with 30 cargos measured in each trial. *P*-values from two-sample Welch's *t*-tests are indicated. (*B*) Tau inhibition of motile fraction was not affected by preincubating microtubules with 100 μM DOPC lipid vesicles (+Vesicles). Tau-decorated microtubules (+Tau) were prepared at an incubation ratio of 0.18 tau per tubulin dimer. Confidence intervals, sample size, and statistical tests are as described in (*A*). These results are consistent with reports that tau binds anionic lipids but not neutral lipids (5) (such as the neutral DOPC lipid used here, Materials and Methods in the main text).

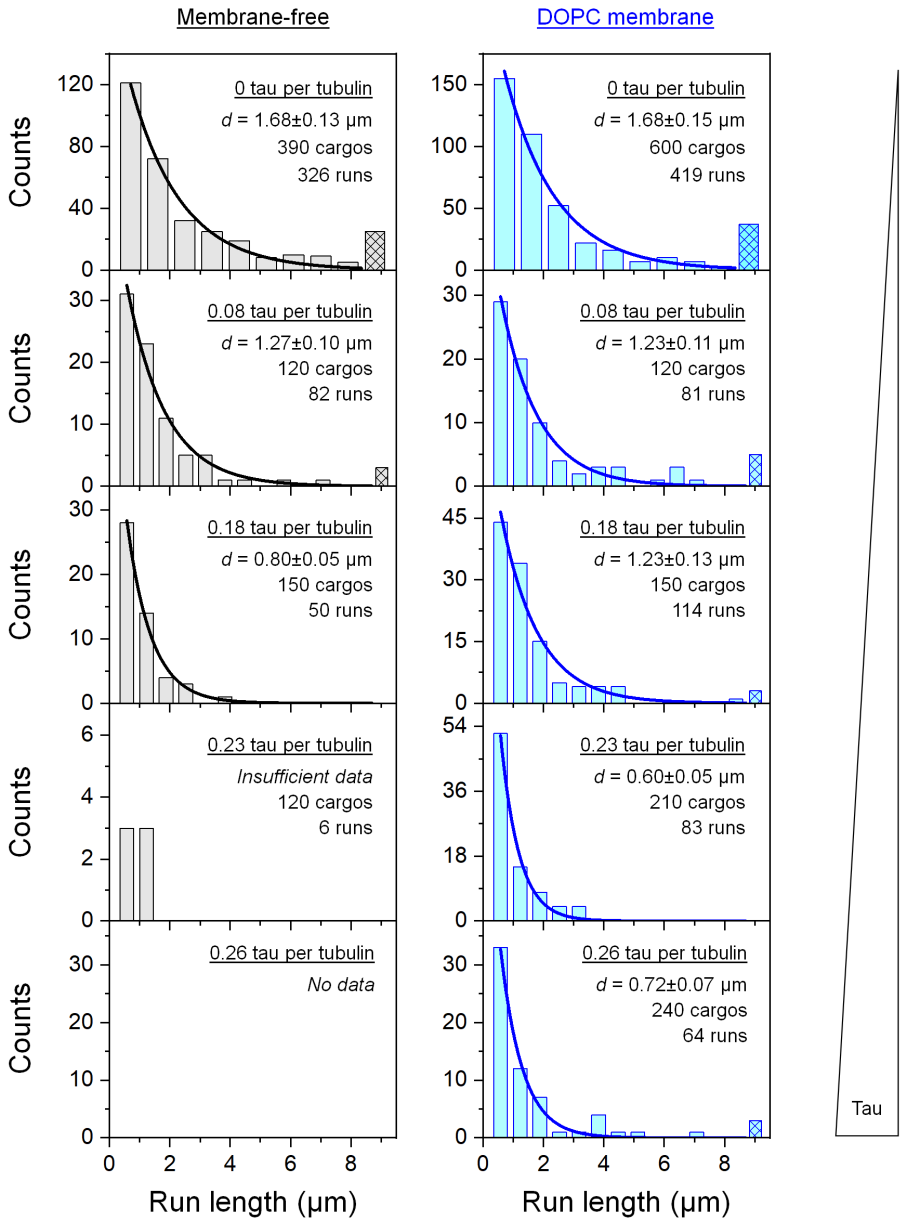

Fig. S2. Run-length distributions of cargos carried by the kinesin heavy chain isoform 5B (Kif5B), corresponding to Figure 1*A* in the main text. Tau concentration, mean run length (*d*, ± standard error of mean (SEM)), number of cargos tested, and number of motile runs are indicated. Solid lines indicate single exponential fits to runs within the experimental field of view. Hatched bars indicate runs that exceeded the field of view.

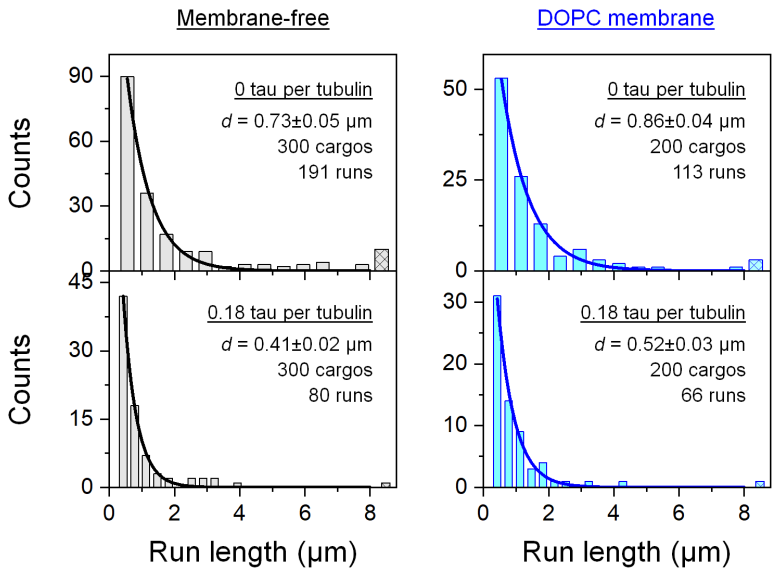

Fig. S3. Run-length distributions of cargos carried by the kinesin heavy chain isoform 5A (Kif5A), corresponding to Figure 1*B* in the main text. Tau concentration, mean run length (*d*, ± SEM), number of cargos tested, and number of motile runs are indicated. Solid lines indicate single exponential fits to runs within the experimental field of view. Hatched bars indicate runs that exceeded the field of view.

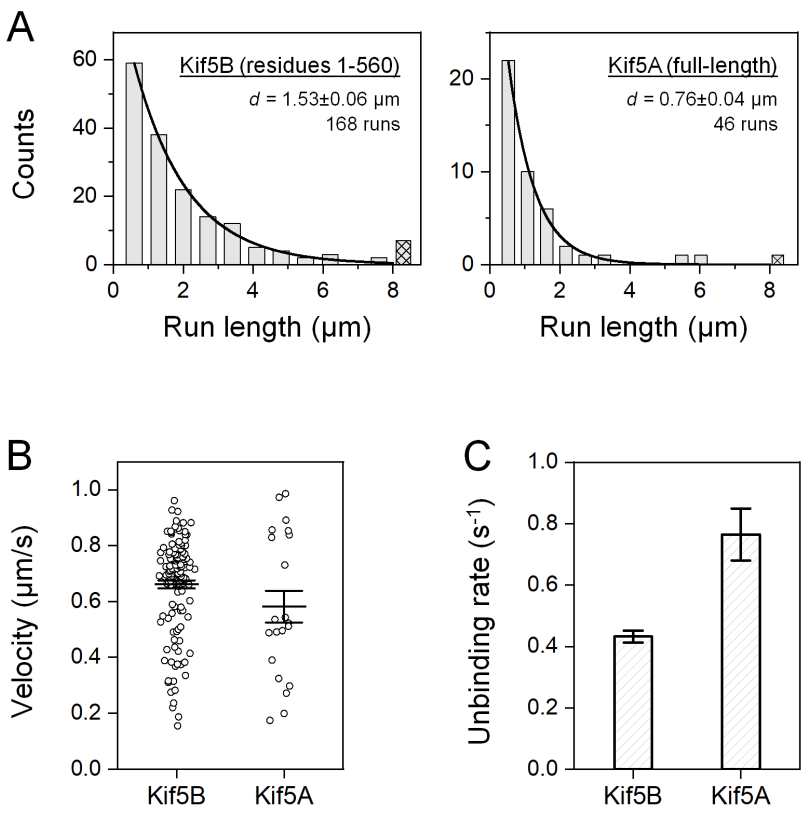

Fig. S4. The neuronal isoform Kif5A unbinds from the microtubule substantially faster than the ubiquitous isoform Kif5B. (*A*) Run-length distributions of membrane-free cargos carried by a single Kif5B or Kif5A in the absence of tau. The concentration of kinesin was tuned such that the fraction of motile cargos in the absence of tau was ~30%, indicating transport by a single motor (1, 2). Mean run length (*d*, ± SEM), number of cargos tested, and number of motile runs are indicated. Solid lines indicate single exponential fits to runs within the experimental field of view. Hatched bars indicate runs that exceeded the field of view. (*B*) Velocity of single kinesins in the absence of tau. Horizontal lines indicate mean and 68% confidence interval. *n* = 139 for Kif5B and 21 runs for Kif5A. (*C*) Unbinding rate of a single kinesin from the microtubule in the absence of tau, determined as the ratio of the mean velocity (*B*) to the mean run length (*A*) for each isoform. Error bars indicate SEM. Kif5A unbinds ~1.8 ± 0.2-fold faster than Kif5B.

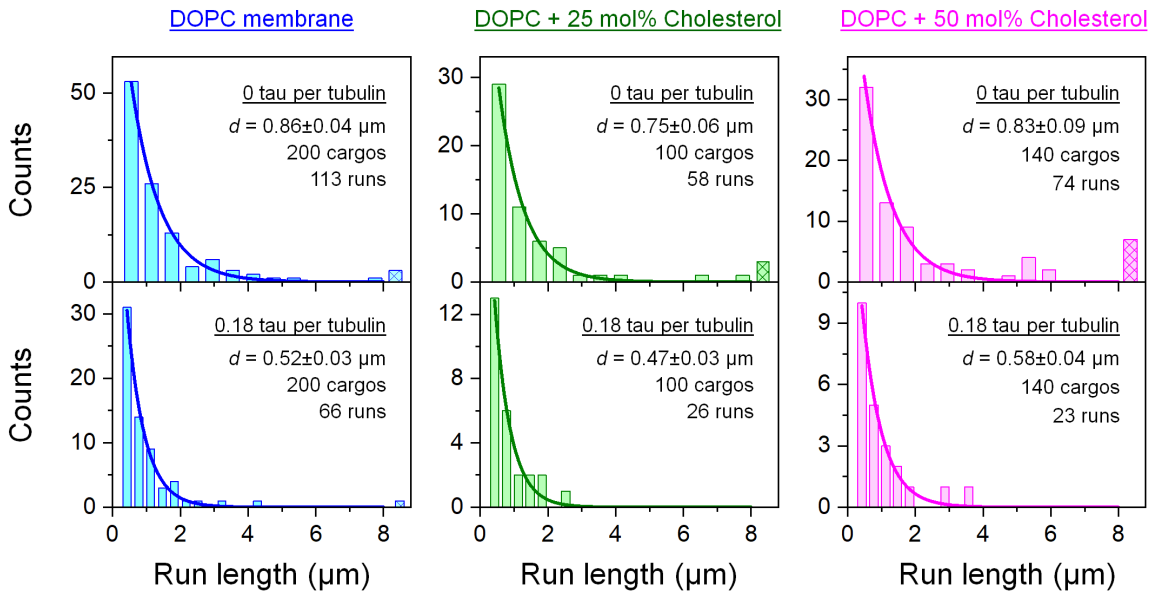

Fig. S5. Run-length distributions of cargos carried by the neuronal isoform Kif5A, corresponding to Figure 2*A* in the main text. The concentration of Kif5A was kept constant at 2.1 nM, corresponding to a motile fraction of ~75% in the absence of tau. Tau concentration, mean run length (*d*, ± SEM), number of cargos tested, and number of motile runs are indicated. Solid lines indicate single exponential fits to runs within the experimental field of view. Hatched bars indicate runs that exceeded the field of view.

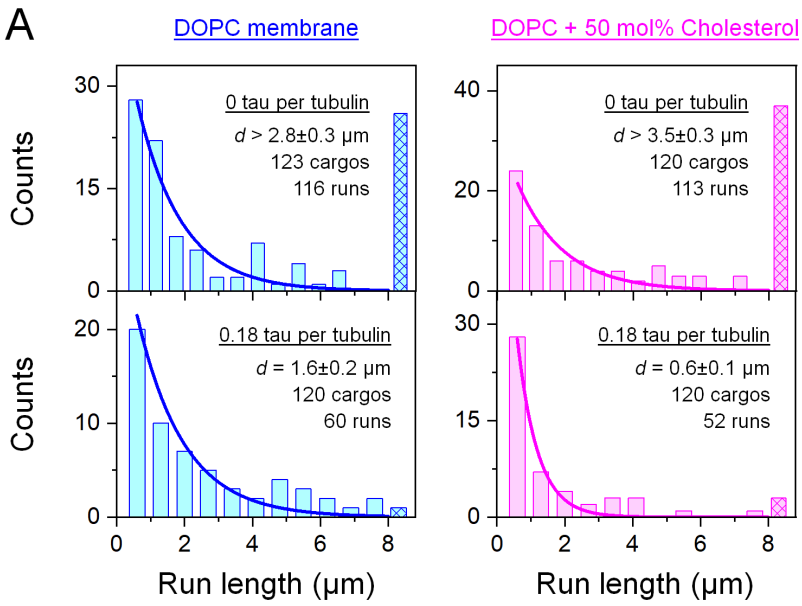

B

Cargo membrane	Tau-free run length		
	12.7 nM Kif5A	Single Kif5A	Fold-increase
DOPC membrane	>2.8±0.3 µm	0.76±0.04 µm	>3.7±0.4 fold
DOPC + 50 mol% cholesterol	>3.5±0.3 µm	0.76±0.04 µm	>4.6±0.5 fold

Fig. S6. Run length of cargos carried by the neuronal isoform Kif5A, corresponding to Figure 2*B* in the main text. The concentration of Kif5A was kept constant at 12.7 nM, corresponding to a motile fraction of 100% in the absence of tau. (*A*) Run-length distributions of motile cargos. Tau concentration, mean run length (*d*, ± SEM), number of cargos tested, and number of motile runs are indicated. Solid lines indicate single exponential fits to runs within the experimental field of view. Membrane cholesterol amplified tau inhibition of run length (P = 0.02, Mann-Whitney U test) but did not impact run length in the absence of tau (P = 0.81, Mann-Whitney U test). Mean run lengths in the absence of tau are lower bound estimates, because a substantial fraction of cargos exceeded the 8-µm field of view (hatched bars). (*B*) The tau-free run lengths (determined in *A*) were >4-fold longer than that of cargos carried by a single Kif5A (determined in Fig. S4*A*). Error bars indicate SEM.

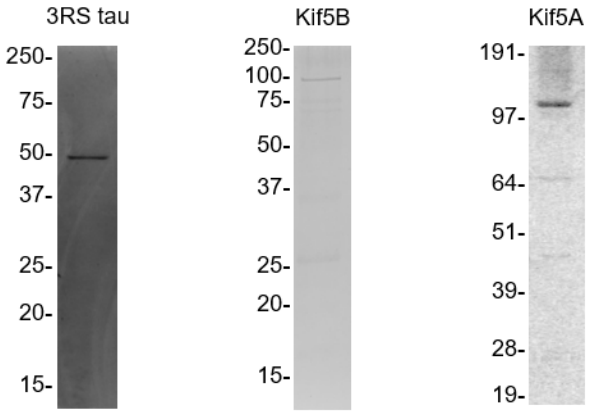

Fig. S7. Representative SDS-PAGE of purified 3RS tau (37 kDa), Kif5B (98 kDa), and Kif5A (117 kDa) proteins. Positions of molecular weight standards (in kDa) are indicated. The mobility of the 3RS tau protein on the SDS-PAGE gel is somewhat larger than its actual molecular weight, this result is consistent with previous reports (6-9). The molecular weight of the Kif5B protein includes that of Kif5B (residues 1-560; 64 kDa), a 33 kDa C-terminal Halo tag, a 697 Da HaloTag PEG-Biotin ligand, and a 244 Da biotin (see Materials and Methods in the main text).

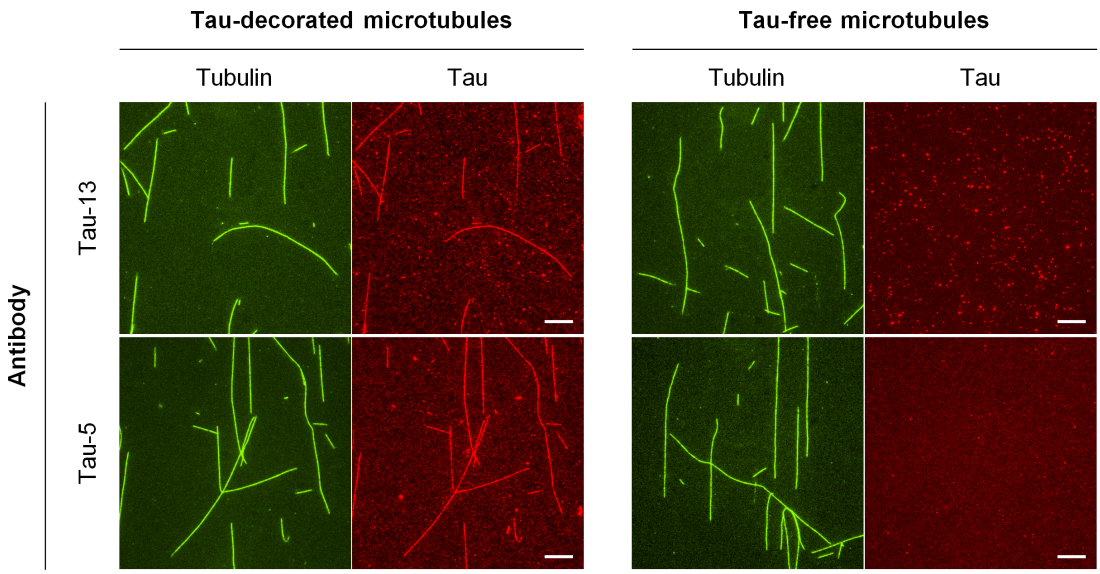

Fig. S8. Tau coverage of *in vitro* microtubules verified via immunostaining. Tau-13, an antibody against the N-terminal region of tau. Tau-5, an antibody against the mid-domain of tau. Tau-decorated microtubules (*Left panels*) immunostained with either a Tau-13 antibody or a Tau-5 antibody revealed nearly perfect co-localization of tau and microtubules. Control experiments using tau-free microtubules (*Right panels*) detected no colocalization of either tau antibody with microtubules and no cross-channel bleed-through. Scale bars, 10 μm.

Movie S1 (separate file). A representative non-motile cargo. *Top*: An optically trapped cargo was positioned near a microtubule for interaction. The cargo did not bind or move directionally away from the trap center. The trap was shuttered after 30 s and the cargo diffused away from the microtubule thereafter. *Bottom*: Position of the cargo as a function of time.

Movie S2 (separate file). A representative motile cargo, corresponding to experiments employing tau-free microtubules and 0 mol% cholesterol in Figure 2A. *Top*: An optically trapped cargo was positioned near a microtubule for interaction. The cargo demonstrated directed motion away from the trap center. The trap was shuttered to measure the zero-load run length. *Bottom*: Position of the cargo as a function of time.

Movie S3 (separate file). A representative motile cargo, corresponding to experiments employing tau-decorated microtubules and 0 mol% cholesterol in Figure 2A. *Inset*: An optically trapped cargo was positioned near a microtubule for interaction. The cargo demonstrated directed motion away from the trap center. The trap was shuttered to the zero-load run length. *Main*: Position of the cargo as a function of time.

Movie S4 (separate file). A representative motile cargo, corresponding to experiments employing tau-free microtubules and 25 mol% cholesterol in Figure 2A. *Inset*: An optically trapped cargo was positioned near a microtubule for interaction. The cargo demonstrated directed motion away from the trap center. The trap was shuttered to measure the zero-load run length. *Main*: Position of the cargo as a function of time.

Movie S5 (separate file). A representative motile cargo, corresponding to experiments employing tau-decorated microtubules and 25 mol% cholesterol in Figure 2A. *Inset*: An optically trapped cargo was positioned near a microtubule for interaction. The cargo demonstrated directed motion away from the trap center. The trap was shuttered to measure the zero-load run length. *Main*: Position of the cargo as a function of time.

Movie S6 (separate file). A representative motile cargo, corresponding to experiments employing tau-free microtubules and 50 mol% cholesterol in Figure 2A. *Top*: An optically trapped cargo was positioned near a microtubule for interaction. The cargo demonstrated directed motion away from the trap center. The trap was shuttered to measure the zero-load run length. *Bottom*: Position of the cargo as a function of time.

Movie S7 (separate file). A representative motile cargo, corresponding to experiments employing tau-decorated microtubules and 50 mol% cholesterol in Figure 2A. *Inset*: An optically trapped cargo was positioned near a microtubule for interaction. The cargo demonstrated directed motion away from the trap center. The trap was shuttered to measure the zero-load run length. *Main*: Position of the cargo as a function of time.

Movie S8 (separate file). A representative motile cargo, corresponding to experiments employing tau-free microtubules and 0 mol% cholesterol in Figure 2B. *Top*: An optically trapped cargo was positioned near a microtubule for interaction. The cargo demonstrated directed motion away from the trap center. The trap was shuttered to the zero-load run length. *Bottom*: Position of the cargo as a function of time.

Movie S9 (separate file). A representative motile cargo, corresponding to experiments employing tau-decorated microtubules and 0 mol% cholesterol in Figure 2B. *Inset*: An optically trapped cargo was positioned near a microtubule for interaction. The cargo demonstrated directed motion away from the trap center. The trap was shuttered to the zero-load run length. *Main*: Position of the cargo as a function of time.

Movie S10 (separate file). A representative motile cargo, corresponding to experiments employing tau-free microtubules and 50 mol% cholesterol in Figure 2B. *Inset*: An optically trapped cargo was

positioned near a microtubule for interaction. The cargo demonstrated directed motion away from the trap center. The trap was shuttered to the zero-load run length. *Main*: Position of the cargo as a function of time.

Movie S11 (separate file). A representative motile cargo, corresponding to experiments employing tau-decorated microtubules and 50 mol% cholesterol in Figure 2B. *Inset*: An optically trapped cargo was positioned near a microtubule for interaction. The cargo demonstrated directed motion away from the trap center. The trap was shuttered to the zero-load run length. *Main*: Position of the cargo as a function of time.

SI References

1. S. M. Block, L. S. Goldstein, B. J. Schnapp, Bead movement by single kinesin molecules studied with optical tweezers. *Nature* **348**, 348-352 (1990).
2. K. Svoboda, S. M. Block, Force and velocity measured for single kinesin molecules. *Cell* **77**, 773-784 (1994).
3. M. T. Gyparaki *et al.*, Tau forms oligomeric complexes on microtubules that are distinct from tau aggregates. *Proc. Natl. Acad. Sci. U.S.A.* **118**, e2021461118 (2021).
4. M. Mikhaylova *et al.*, Resolving bundled microtubules using anti-tubulin nanobodies. *Nat. Commun.* **6**, 7933 (2015).
5. E. M. Jones *et al.*, Interaction of tau protein with model lipid membranes induces tau structural compaction and membrane disruption. *Biochemistry* **51**, 2539-2550 (2012).
6. M. Vershinin, B. C. Carter, D. S. Razafsky, S. J. King, S. P. Gross, Multiple-motor based transport and its regulation by Tau. *Proc. Natl. Acad. Sci. U.S.A.* **104**, 87-92 (2007).
7. N. V. Gorantla, P. Khandelwal, P. Poddar, S. Chinnathambi, Global Conformation of Tau Protein Mapped by Raman Spectroscopy. *Methods Mol. Biol.* **1523**, 21-31 (2017).
8. H. A. Weismiller *et al.*, Structural disorder in four-repeat Tau fibrils reveals a new mechanism for barriers to cross-seeding of Tau isoforms. *J. Biol. Chem.* **293**, 17336-17348 (2018).
9. R. Tan *et al.*, Microtubules gate tau condensation to spatially regulate microtubule functions. *Nat. Cell Biol.* **21**, 1078-1085 (2019).